ACS Catalysis

Research Article

pubs.acs.org/acscatalysis

Tunable KIT-6 Mesoporous Sulfonic Acid Catalysts for Fatty Acid Esterification

Cyril Pirez, Jean-Michel Caderon, Jean-Philippe Dacquin,† Adam F. Lee, and Karen Wilson*

Cardiff Catalysis Institute, School of Chemistry, Cardiff University, Park Place, Cardiff CF10 3AT, U.K.

Supporting Information

ABSTRACT: We report the first catalytic application of pore-expanded KIT-6 propylsulfonic acid ($PrSO_3H$) silicas, in fatty acid esterification with methanol under mild conditions. As-synthesized $PrSO_3H$-KIT-6 exhibits a 40 and 70% enhancement in turnover frequency (TOF) toward propanoic and hexanoic acid esterification, respectively, over a $PrSO_3H$-SBA-15 analogue of similar 5 nm pore diameter, reflecting the improved mesopore interconnectivity of KIT-6 over SBA-15. However, pore accessibility becomes rate-limiting in the esterification of longer chain lauric and palmitic acids over both solid acid catalysts. This problem can be overcome via hydrothermal aging protocols which permit expansion of the KIT-6 mesopore to 7 nm, thereby doubling the TOF for lauric and palmitic acid esterification over that achievable with $PrSO_3H$-SBA-15.

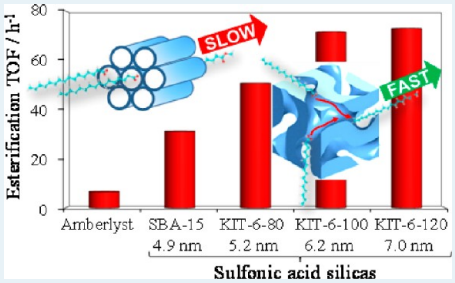

KEYWORDS: *biodiesel, nanostructured silicas, green chemistry, solid acids, esterification*

1. INTRODUCTION

Concerns over dwindling fossil fuel reserves, coupled with rising atmospheric CO_2 emissions, is helping to drive the renewable energy revolution and the associated promise of lower greenhouse gas emissions. Wind, solar, and tidal energy resources are all potential alternatives for stationary power generation;[1] however, liquid biofuels are one of the few competitors to petroleum able to contribute to transportation needs, with ~9% of the transportation fuel market predicted to be met through biofuels by 2030.[2]

Biodiesel, comprising fatty acid methyl esters (FAMEs)[3] produced via the transesterification of triacyl glycerides from nonfood oil sources, is an attractive and (potentially) sustainable means to reduce current fossil fuel dependency, and is seeing a renaissance following steeply rising petroleum costs. However, current industrial biodiesel production is neither energy efficient nor environmentally friendly.[4] Although the commercial homogeneous base catalysts employed, Na or K methoxide, are very active for such transesterification, the strict guidelines on residual alkali content in biofuel at <5 ppm,[5,6] necessitate thorough aqueous quench and neutralization steps, with associated soap formation making biodiesel separation energy intensive.[7] Furthermore, plant, algal, and waste oil feedstock pretreatments are essential to remove free fatty acid (FFA) impurities,[8] which are also strictly regulated in biodiesel, and can neutralize soluble base catalysts resulting in soap formation. New heterogeneous catalysts are thus required at various stages in biodiesel production to improve energy efficiency, and permit facile catalyst separation and continuous process operation.[9]

Esterification is widely used to remove FFAs,[10] which are particularly prevalent in waste oils and grease (up to 10−33%).[11] Fatty acid esterification has been studied over many solid acid catalysts, including SO_4/ZrO_2,[12−14] Cs-exchanged heteropolyacids,[15−19] tungstated zirconia,[20] zirconium phosphate[21−23] and Nafion/SiO_2 composite (SAC-13).[24] Poor mass-transport in these systems has focused recent attention on mesporous solid acids,[25] with SBA-15 derived catalysts proving popular candidates for biodiesel synthesis. Indeed, SBA-15 supported propylsulfonic and arylsufonic acids exhibit promising activity in FFA esterification[26−30] and in the esterification of shorter chain acids pertinent to pyrolysis oil pretreatment[31] wherein high acid contents hinder refining.

We recently demonstrated that macropore incorporation[32] into mesoporous SBA-15 sulfonic acids, or swelling of SBA-15 mesopores,[33] significantly enhances activity toward both FFA esterification and triglyceride transesterification. In the case of macro-mesoporous SBA-15, inclusion of 300 nm macropores fractures the micrometer-long, parallel mesopore channels normally present within SBA-15, promoting in-pore molecular diffusion and active site accessibility. Improving pore interconnectivity, for example, through the $Ia\bar{3}d$ pore architecture of KIT-6,[34] could provide another means to enhance pore accessibility (Scheme 1). KIT-6 mesoporous materials exhibit improved characteristics for biomolecule immobilization (e.g., enzymes),[35] related to better diffusion within the interconnected cubic structure. Interconnected silica supports also significantly enhance the per-site activity of Pd nanoparticles in allylic alcohol selective oxidation, wherein Pd/KIT-6 is far superior to Pd/SBA-15.[36] We therefore hypothesized that sulfonic acid functionalization of KIT-6, and expanded variants thereof, may offer tailored solid acid

Received: March 9, 2012
Revised: June 20, 2012
Published: June 21, 2012

Scheme 1. Diagram of (a) SBA-15 and (b) KIT-6 Unit Cells

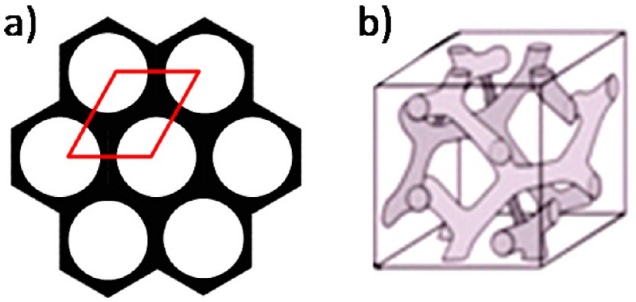

catalysts for the diffusion of bulky FFA molecules during esterification pretreatments employed in biodiesel production. While pore-expanded KIT-6 materials have been previously synthesized,[37] they have never been exploited in heterogeneous catalysis. Surface grafting and oxidation of mercaptopropyl trimethoxysilane to propylsulfonic acid ($PrSO_3H$) was selected as a means to conformally functionalize the different silica pore architectures to introduce acidic groups without the risk of pore blockage or leaching of the grafted component. Here we report on the first synthesis and application of $PrSO_3H$-KIT-6 materials with tunable pore diameters, and compare their performance in C3-16 organic acid esterification against a conventional $PrSO_3H$-SBA-15 catalyst, to identify the impact of pore interconnectivity and diameter.

2. EXPERIMENTAL SECTION

Catalyst Preparation. SBA-15 and KIT-6 materials were prepared following the methods of Zhao et al.[38] and Ryoo et al.,[39] respectively. SBA-15 was prepared using 1.0 g of Pluronic P123 triblock copolymer (Aldrich), which was dissolved in 7.5 mL of water and 25 mL of 2 M HCl solution (Fisher) while stirring at 35 °C. A 2.3 mL portion of TEOS (tetraethoxyorthosilane - Aldrich 99%) was then added to the solution, which was maintained at 35 °C for 24 h while stirring. The mixture was then aged statically at 80 °C for a further 24 h in a closed propylene bottle after which the solid product filtered, washed 3 times with deionized water, and calcined in air at 550 °C for 6 h. For the synthesis of the parent KIT-6 materials 4 g of Pluronic P123 (Aldrich) was dissolved in 144 g of distilled water containing 7.5 g of a solution of 36% HCl. Once a homogeneous solution was formed, 4 g of butanol was added under stirring at 35 °C. After 1 h, 8.6 g of TEOS was added at 35 °C such that a molar ratio of components of 0.017 P123:1 TEOS:1.31BuOH:1.83 HCl:195 H_2O was employed. The mixture was then stirred for 24 h at 35 °C, and subsequently aged for a further 24 h at 80, 100, or 120 °C under static conditions in a closed propylene bottle to vary the mesopore dimensions. Finally the solid product obtained was filtered and dried at 100 °C for 12 h after which the template was removed by calcination at 550 °C for 6 h.

After calcination, silicas were functionalized with sulfonic acid groups by postgrafting, in which 1 g of KIT-6 (or SBA-15) was added to a solution containing 1 mL of mercaptopropyl trimethoxysilane (MPTS 95%, Alfa Aesar) in 30 mL of toluene (Fisher 99%). The suspension was then refluxed at 130 °C under stirring for 24 h, after which the resulting thiol-functionalized solid was filtered, washed three times with methanol (Fisher 99%) and dried at 80 °C overnight. Thiol groups were converted into $-SO_3H$ by mild oxidation with 30 mL of 30% hydrogen peroxide (Sigma-Aldrich) by continuous stirring at room temperature for 24 h. The sulfonated solid product was subsequently filtered, washed three times with methanol, and dried at 80 °C. Materials were stored in air and used without further modification.

Catalyst Characterization. Textural and structural properties were measured by a combination of N_2 porosimetry, transmission electron microscopy (TEM), and X-ray diffraction (XRD), with pre- and postoxidation sulfur content determined by thermogravimetric analysis (TGA, bulk) and X-ray photoelectron spectroscopy (XPS, surface), with acid site titrations performed by NH_3 pulse chemisorption.

Nitrogen porosimetry was undertaken on a Quantachrome Nova 1200 porosimeter, with samples degassed at 120 °C for 2 h prior recording adsorption/desorption isotherms. Brunauer–Emmett–Teller (BET) surface areas were calculated over the relative pressure range 0.01–0.2, while pore diameters were calculated by applying the Barrett–Joyner–Halenda (BJH) method to the desorption branch of the isotherm. Low angle XRD patterns were recorded on a PANalytical X'pertPro diffractometer fitted with an X'celerator detector and Cu Kα (1.54 Å) source. Low angle diffraction peaks were recorded over the range 2θ = 0.3–8° with a step size of 0.01° and calibrated against a Si standard. TEM images were viewed with a Phillips CM12 transmission electron microscope operating at 100 kV. Images recorded by a SIS MegaView III digital camera, with the data analyzed using ImageJ software. Scanning electron microscopy-energy dispersive X-ray (SEM/EDX) was performed with a Carl Zeiss Evo-40 instrument, with samples mounted on conductive carbon tape. XPS was performed on a Kratos Axis HSi instrument fitted with a charge neutralizer and magnetic focusing lens employing Al Kα monochromated radiation (1486.7 eV). Spectral fitting was performed using CasaXPS version 2.3.14, with binding energies corrected to the C 1s peak at 284.5 eV, with S 2p XP spectra fitted using a common Gaussian/Lorentzian peak shape. Errors were estimated by varying the Shirley background-subtraction procedure across reasonable limits and recalculating the component fits. TGA was performed using a Stanton Redcroft STA780 thermal analyzer at 10 °C.min^{-1} under flowing He (20 mL min^{-1} total) for hydroxyl group density and sulfonic acid decomposition studies respectively.

Acid site titration was performed on a Quantachrome CHEMBET-3000 instrument by pulse chemisorption, using pure NH_3 (BOC 99.98%). ~50 mg of catalyst was outgassed at 150 °C for 2 h under flowing He, after which NH_3 adsorption was performed at 100 °C to prevent NH_3 physisorption on the silica surface. Titration was performed by injecting 500 μL pulses of NH_3 with a gas syringe until the detector signal in both TCD and mass spectrometer reached a plateau, indicating that the acid sites were saturated.

Catalytic Esterification. Esterification was performed under stirred batch conditions at atmospheric pressure in a Radley's carousel reaction station using 25 mm diameter glass reactor vessels. Reactions were conducted using 10 mmol propanoic, hexanoic, lauric, or palmitic acid at 60 °C in 12.5 mL of methanol (molar ratio n_{MeOH}/n_{acid} = 30 under which conditions the organic acid and methanol were completely miscible) with 50 mg of catalyst and 0.59 mL of dihexylether as an internal standard. Reaction profiles were obtained via periodic sampling and off-line GC analysis, with product calibration curves used to verify mass balances (all >98%). C_3 and C_6 acid esterification was monitored using a Varian 450-GC equipped with a CP-Sil 5 CB 15 m × 0.25 mm × 0.25 μm

dx.doi.org/10.1021/cs300161a | ACS Catal. 2012, 2, 1607–1614

capillary column. C_{12} and C_{16} acid esterification was followed using a Varian 450-GC equipped with a 1079 programmable direct on-column injector and Phenomenex capillary column ZB-1HT Inferno 15 m × 0.53 mm × 0.15 μm wide bore column. Dichloromethane was used as solvent to dilute the samples for GC analysis. All catalytic profiles are an average of two separate runs with 3 injections per sample. Turnover frequencies (TOF) were determined from the linear portion of the initial reaction rate profile for conversions below 25%, which were normalized to the acid site concentration determined from NH_3 titrations. Leaching studies were performed by hot filtration methods with the reaction stopped and the catalyst removed by filtration at 2 h, after which the reactants were reheated and further conversion monitored for an additional 6 h. For benchmarking catalyst activity is also compared against a commercial Amberlyst 15 hydrogen form (Fluka) strongly acidic macro-reticular resin with particle size 600−850 μm and acid site loading 4.7 mmol/g.

3. RESULTS AND DISCUSSION

Materials Characterization. Successful synthesis of SBA-15 and pore-expanded KIT-6 parent silicas was confirmed by XRD, TEM, and porosimetry. Figure 1 shows the correspond-

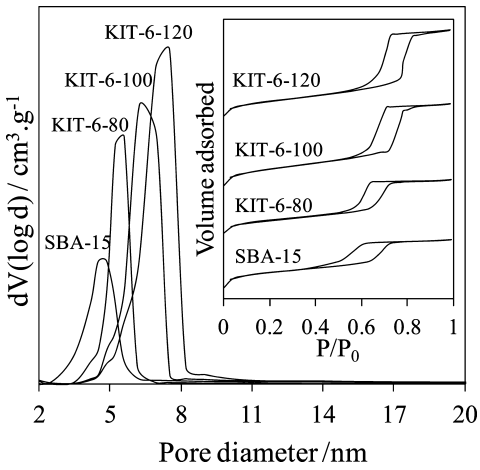

Figure 1. Main: pore size distributions of parent SBA-15 and KIT-6 mesoporous silicas. Inset: associated N_2 adsorption−desorption isotherms (offset for clarity).

ing N_2 isotherms and BJH pore size distributions, which reveal all silicas exhibit Type IV isotherms with H1 hysteresis loops[40] characteristic of open cylindrical pores (Figure 1 inset). BJH analysis on the desorption branch of the isotherm confirms they all possess well-defined mesopore diameters, which increase with KIT-6 hydrothermal aging temperature from 80 to 120 °C. It should be noted that the hysteresis loop for KIT-6 is narrower than that of SBA-15, which has been attributed to the influence of mesopore interconnectivity on N_2 vaporization.[40] This different hysteresis behavior is thus a characteristic of their 2D hexagonal (SBA-15) versus 3D cubic (KIT-6) structures.

HRTEM and XRD were used to confirm the gyroidal cubic $Ia\bar{3}d$ and *p6mm* hexagonal structures (Scheme 1) and typical lattice parameters of KIT-6 and SBA-15 respectively. Low angle XRD in Figure 2 shows the characteristic d_{100}, d_{110}, and d_{200} planes typical of the 2D hexagonal structure in SBA-15, and the d_{112} plane of the 3D gyroidal KIT-6. The d_{112} reflection shifts to lower angle with increasing aging temperature, consistent with

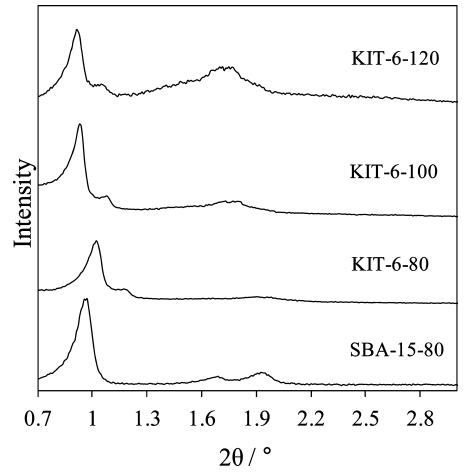

Figure 2. Powder XRD patterns of parent SBA-15 and KIT-6 mesoporous silicas.

an increase in the unit cell parameter, and corresponding pore spacing. The unit cell of SBA-15 is expected to be around half that of KIT-6, consistent with our measurements summarized in Table 1 along with those from porosimetry. The SBA-15 benchmark support has a specific area of 862 $m^2\ g^{-1}$, significantly higher than that of our conventional KIT-6 material aged at 80 °C; however, they possess similar BJH pore diameters of 4.9 and 5.2 nm respectively. Hydrothermal aging of KIT-6 at 100 and 120 °C expands the pore diameter from 5.2 to 7 nm, while decreasing wall thickness, in line with literature predictions.[41,42] To date, increasing the hydrothermal aging temperature/time has proven the only method to increase KIT-6 pore size; attempts to use porogens such as trimethylbenzene as a micelle expander have only resulted in amorphous materials.[37]

Sulfonic acid derivatized $PrSO_3H$-KIT-6 and $PrSO_3H$-SBA-15 materials were subsequently prepared via grafting of MPTS and oxidation with H_2O_2. This is the first report of $PrSO_3H$-KIT-6; hence the support stability postgrafting was verified by XRD, porosimetry, and HRTEM to ensure the cubic structure was retained (Figure 3 and Supporting Information, Figures S1−S2). HRTEM shown in Figure 4 confirms the cubic architecture of KIT-6 silicas is retained both upon expansion and grafting of sulfonic acid groups. The conformal nature of this surface modification method is further evidenced by the textural analysis in Table 2, which shows only a slight decrease in surface area following grafting of sulfonic acid groups.

Sulfur 2p XP spectra (Figure 5) only exhibit a single doublet centered at 169 eV, indicative of complete oxidation of the grafted thiol groups to sulfonic acid, which is also consistent with TGA measurements that show a single decomposition step ∼450 °C characteristic of propylsulfonic acid group decomposition.[43] Comparison of the bulk and surface S contents demonstrates a higher sulfonic acid loading is achieved on SBA-15 than across the KIT-6 family, suggesting a higher density of reactive silanol groups in the former, which may reflect their different aging conditions and surface roughness. TGA analysis (Supporting Information, Figure S4) was used to estimate the surface hydroxyl loadings of the as-prepared silica,[44] which yields values ∼3.3 and 2.2 mmol g^{-1} for SBA-15 and KIT-6-80, respectively. While this assumes the weight loss in this temperature range 200−400 °C is entirely due to 2 Si−OH → Si−O−Si + H_2O, the values obtained broadly support

dx.doi.org/10.1021/cs300161a | ACS Catal. 2012, 2, 1607−1614

Table 1. Structural Parameters for Parent KIT-6 and SBA-15 Supports

catalyst	surface area[a]/ $m^2\ g^{-1}$	pore volume/ $cm^3\ g^{-1}$	BJH pore diameter[b]/ nm	plane spacing[c]/ nm	unit cell parameter[d]/ nm	wall thickness[e]/ nm	TEM pore spacing/ nm
KIT-6-80	601	0.83	5.2	8.65	21.2	5.4	7.9
KIT-6-100	661	1.23	6.2	9.5	23.2	5.4	8.3
KIT-6-120	676	1.29	7.0	9.7	23.7	4.9	9.1
SBA-15	862	0.77	4.9	9.20	10.7	6.1	8.2

[a]From BET. [b]Analyzed from the desorption branch. [c]From Braggs law assuming that the peak corresponds to the (100) plane for SBA-15 and (211) plane for KIT-6. [d]For SBA-15 = $a_0 = (2d_{100})/\sqrt{3}$; for KIT-6 = $(d_{211}) \times \sqrt{6}$; [e]For SBA-15 = ($a$ - pore diameter); for KIT-6 = ($a/2$ - pore diameter) based on unit cell.

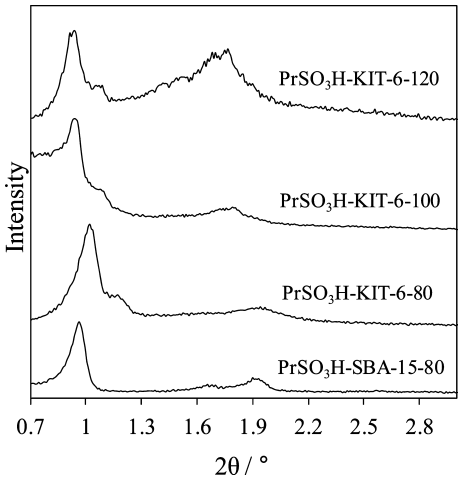

Figure 3. Powder XRD patterns for the sulfonic acid derivatized SBA-15 and KIT-6 mesoporous silicas.

the hypothesis that the hydroxyl density in SBA-15 > KIT-6. Acid site densities from NH_3 pulse chemisorption (Table 2) mirror the trends in bulk and surface S loadings observed by TGA and XPS, and are typical of grafted sulfonic acid silicas which range between 0.1 and 1 mmol g^{-1}.[26]

Catalytic Esterification. Sulfonic-acid grafted silicas were subsequently evaluated in propanoic (C_3), hexanoic (C_6), lauric (C_{12}), and palmitic (C_{16}) acid esterification with methanol at 60 °C to assess the interplay between catalyst pore diameter, pore architecture, and organic acid chain length on activity (Supporting Information, Figures S5–S9). Representative reaction profiles for the $PrSO_3H$-KIT-6-80 and $PrSO_3H$-KIT-6-120 samples, possessing 5.2 and 7.0 nm pores, are shown in Figure 6. Although both catalysts show slower initial rates and lower conversions with increasing acid chain length, the relative drop in performance of the larger pore $PrSO_3H$-KIT-6-120 is slight compared with that of $PrSO_3H$-KIT-6-80 which is very poor for lauric and palmitic acid. This suggests that significant mass-transport limitations can be important for relatively small fatty acids (>C_6), even when relatively large (5 nm) porous catalysts are employed. However, slight pore-expansion can prove sufficient to alleviate these diffusional effects.

A general decrease in esterification rate with alkyl chain length is of course expected, and previously reported in C_2–C_8 acid esterification using both H_2SO_4 and silica/Nafion composite SAC-13.[45] Such decreases are attributed to a combination of polar and steric influences of the alpha substituent on the carboxylic group. Inductive effects may decrease reactivity; while the carboxylate electron density increases with alkyl chain length, favoring initial protonation, the electrophilicity of the carbonyl simultaneously decreases, thus disfavoring subsequent alkoxy insertion.[45] Above C_4 chain length, electronic properties are not believed to significantly evolve; hence, subsequent variations in rate are attributed to steric or mixing effects, the former predicted via the Taft equation. Previous groups have shown a linear correlation between Taft parameter and rates for C_2–C_8 acids;[46,45] however >C_8 the Taft parameter remains constant.[47] Steric and bulk mixing effects are expected to be more significant for longer chains, wherein conformational changes are likely to minimize the interfacial energy between the hydrophobic alkyl chain and polar methanol solvent. For homogeneous catalysts, the impact of such a change in fatty acid "bulkiness" may be negligible; however, for a nanoporous catalyst it seems probable that it would alter in-pore diffusion, leading to the poor performance of $PrSO_3H$-KIT-6-80.

The effect of interconnectivity and pore expansion on catalyst performance was assessed by comparing the $PrSO_3H$-KIT-6 family with $PrSO_3H$-SBA-15 and a commercial macroreticular Amberlyst-15 solid acid catalyst in Figure 7. The first striking observation is that while higher overall conversions are possible with Amberlyst because of its higher acid site loading (Supporting Information, Figure S9a), both SBA-15 and KIT-6 sulfonic acid silicas significantly outperform Amberlyst in terms of per site activity, reflecting the low porosity and accessibility of acid sites within the polymeric catalyst. $PrSO_3H$-KIT-6-80 also outperforms $PrSO_3H$-SBA-15 in C_3 and C_6 acid esterification, despite their similar pore diameters, suggesting the improved pore interconnectivity of the former enhances reactant/product diffusion. Although these values are substantially lower than those reported for H_2SO_4 catalyzed propanoic acid and hexanoic acid esterification at 60 °C of 727 h^{-1} and 478.8 h^{-1}, respectively, a similar ∼30% decrease in TOF is observed between the C_3 and C_6 acids in these homogeneously catalyzed systems, hinting that solution phase properties play an important part in controlling our reaction kinetics. Corresponding values of 285 h^{-1} and 133 h^{-1} are reported for SAC-13 catalyzed C_3 and C_6 organic acid esterification,[45] slightly higher than those reported here for our $PrSO_3H$-KIT-6 and $PrSO_3H$-SBA-15 catalysts reflecting the stronger acidity of SAC-13: NH_3 calorimetry gives adsorption enthalpies of −158 kJ mol^{-1} and −130 kJ mol^{-1} respectively for Nafion and $PrSO_3H$-SBA-15.[48] The impact of acid strength on acetic acid esterification has been demonstrated by comparing the rates for homogeneous propane sulfonic acid (264 h^{-1}) versus H_2SO_4 (1365 h^{-1}) catalysts.[49] Likewise, the reported TOF for acetic acid esterification with methanol of 436 h^{-1} over SAC-13 is higher than the 180 h^{-1} for $PrSO_3H$-SBA-15, with both slower than homogeneous routes. Although acid strength clearly influences esterification activity,[50] our best $PrSO_3H$-KIT-6-120 solid acid measures up favorably against its liquid phase propyl-sulfonic acid analogue. Subsequent leaching tests via hot-filtration shown in Supporting Information, Figure S9 for hexanoic acid

dx.doi.org/10.1021/cs300161a | ACS Catal. 2012, 2, 1607–1614

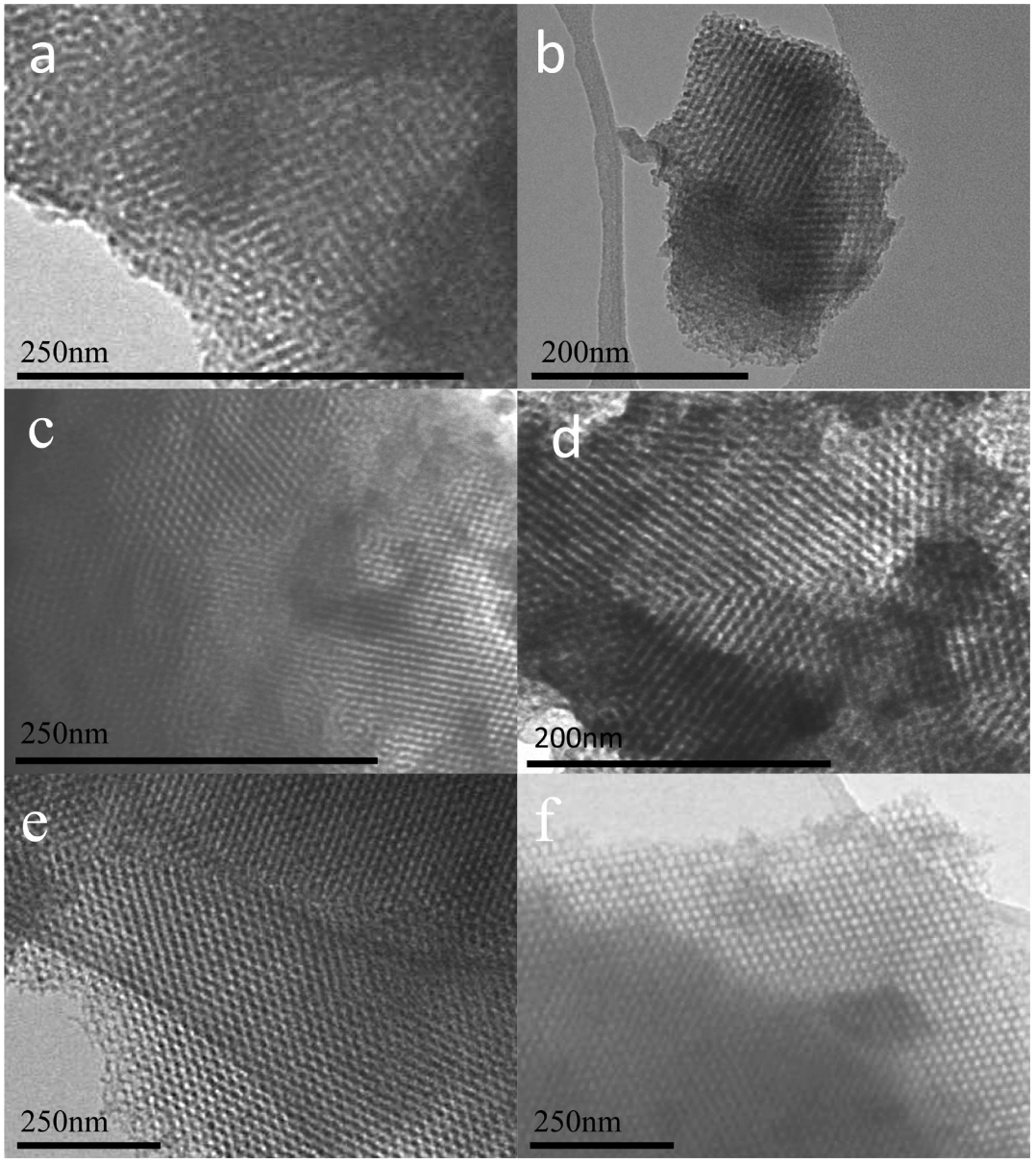

Figure 4. TEM images of parent and sulfonated KIT-6 silicas; (a) KIT-6-80, (b) $PrSO_3H$-KIT-6-80, (c) KIT-6-100, (d) $PrSO_3H$-KIT-6-100, (e) KIT-6-120, (f) $PrSO_3H$-KIT-6-120.

Table 2. Surface and Bulk Properties of KIT-6 and SBA-15 Sulphonic Acid Silicas

catalyst	surface area[a]/ $m^2\ g^{-1}$	BJH pore diameter[b]/ nm	plane spacing/ nm	unit cell parameter/ nm	wall thickness/ nm	bulk S content[c]/ wt %	surface S content[d]/ wt %	acid site loading[e]/ mmol g^{-1}	acid site density/H^+ nm^{-2}
$PrSO_3H$-KIT-6-80	540	5.2	8.6	21.1	5.3	0.74	0.66	0.32	0.35
$PrSO_3H$-KIT-6-100	539	6.2	9.4	23.0	5.3	0.73	0.73	0.25	0.28
$PrSO_3H$-KIT-6-120	546	7.0	9.5	23.3	4.7	0.72	0.69	0.38	0.42
$PrSO_3H$-SBA-15−80	813	4.9	9.2	10.6	6.1	1.12	0.95	0.67	0.49

[a]From BET equation. [b]Analyzed from the desorption branch. [c]Bulk S content from TGA (weight loss between 450−600 °C). [d]Surface S content from XPS. [e]Based on NH_3 chemisorption (accurate to ±0.05 $mmolg^{-1}$).

esterification also verify the stability of the grafted acid sites on both $PrSO_3H$-SBA-15 and $PrSO_3H$-KIT-6-120 under the mild operating conditions employed in this study.

Figure 8 shows the relative performance of $PrSO_3H$-KIT-6 catalysts versus $PrSO_3H$-SBA-15. The enhanced performance of $PrSO_3H$-KIT-6-80, apparent for propanoic and hexanoic acids, is lost >C_6, consistent with limited in-pore accessibility for both 5 nm architectures. Pore expansion mitigates this problem, with $PrSO_3H$-KIT-6-100 and $PrSO_3H$-KIT-6-120 exhibiting a monotonic improvement over $PrSO_3H$-SBA-15 with increasing alkyl chain length, conferring a 2-fold rate enhancement for palmitic acid esterification. Table 3 compares palmitic acid esterification TOFs over different sulfonic acid silicas, and demonstrates that our new $PrSO_3H$-KIT-6 solid acid catalysts

dx.doi.org/10.1021/cs300161a | ACS Catal. 2012, 2, 1607−1614

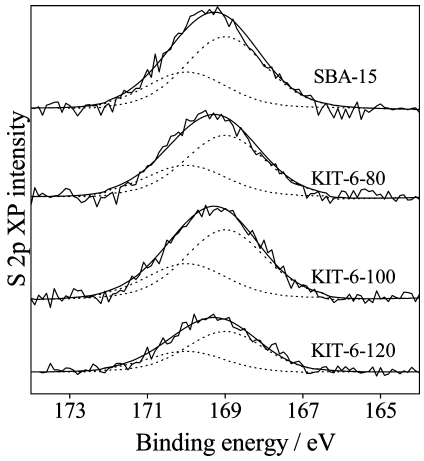

Figure 5. S 2p XP spectra of propyl sulfonic acid derivatized SBA-15 and KIT-6 catalysts (fitted spin−orbit doublet shown as dotted lines).

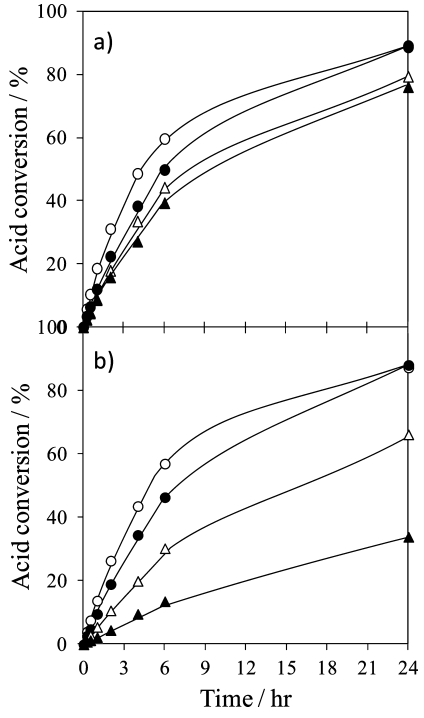

Figure 6. Reaction profiles for (○) propanoic, (●) hexanoic, (Δ) lauric, and (▲) palmitic acid esterification with methanol at 60 °C over (a) $PrSO_3H$-KIT-6-120 and (b) $PrSO_3H$-KIT-6-80.

consistently outperform their $PrSO_3H$-SBA-15 counterparts possessing similar pore diameters, despite possessing similar acid strengths. Since the TOF should be a constant if the intrinsic reaction kinetics of a unique active site (e.g., a sulfonic acid moiety) are measured, the observed variation in Table 3 suggests that other factors relating to the pore architecture play an important role in regulating fatty acid esterification. SBA-15 crystallites exhibit a high aspect ratio of approximately 60 × 6 μm (Supporting Information, Table S1, Figure S11) reflecting the many micrometer-length, parallel pore channels spanning the longer axis. In such a morphology, pore entrances preferentially dominate the smaller end faces, giving rise to a net low number of openings averaged across the entire crystallite volume (~290 pore entrances.μm^{-3} for the crystallite dimensions in this study). [Calculated for a 61 × 6.5 × 6.5 μm

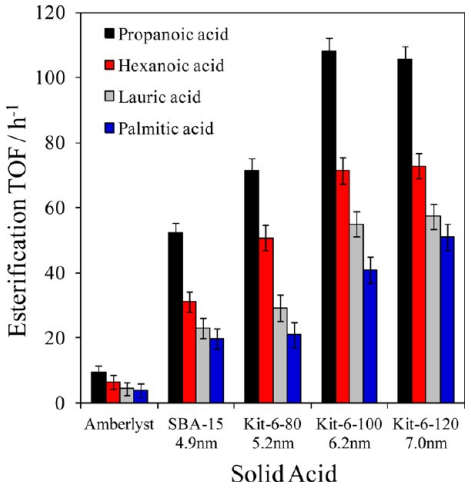

Figure 7. Comparative performance of $PrSO_3H$-SBA-15 and $PrSO_3H$-KIT-6 series versus Amberlyst 15 in propanoic, hexanoic, lauric, and palmitic acid esterification with methanol at 60 °C.

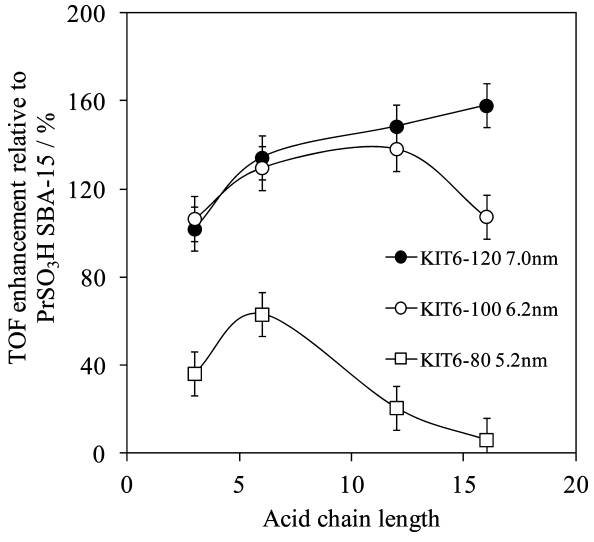

Figure 8. Relative performance of $PrSO_3H$-KIT-6 versus $PrSO_3H$-SBA-15 in fatty acid esterification with methanol at 60 °C as a function of acid chain length.

SBA-15 crystal or a 8.4 × 8.4 × 8.4 μm KIT-6 crystal, assuming 1 pore per face of the SBA-15 unit cell and 4 pores per face of the KIT-6 unit cell as shown in Scheme 1.] In contrast, the three-dimensional nature of KIT-6 affords access to the interior of crystallites via pore entrances uniformly distributed across the *entire external surface*, providing far higher accessibility (~6400 pore entrances μm^{-3} for our KIT-6-80 crystallites), which we believe contributes to the superior performance observed in the present study. A consequence of these differing pore architectures is that decreasing the length of pore channels within SBA-15 crystallites can dramatically enhance the surface density of pore openings (confined to the end faces) relative to the crystallite volume, and thus accessibility of the porous interior, resulting in significant rate-enhancements as observed for platelet-like SBA-15 with short (150−350 nm) meso-channels toward fatty acid esterification.[51] Mechanical grinding of SBA-15 to reduce their pore channel length confers similar catalytic promotion.[52] We are currently undertaking molecular dynamics simulations to better understand and optimize FFA

dx.doi.org/10.1021/cs300161a | *ACS Catal.* 2012, 2, 1607−1614

Table 3. Palmitic Acid Conversion and Turnover Frequencies (TOFs) for KIT-6 and SBA-15 Sulfonic Acid Silica

catalyst	pore diameter /nm	acid conv.[a] /%	TOF[b] /h^{-1}	TOF[c] /h^{-1}	reference
Amberlyst-15	na	45.0	3.6	na	this work
$PrSO_3H$-SBA-15	4.9	35.6	19.7	34.1	this work
$PrSO_3H$-KIT-6-80	5.2	13.6	21.0	33.2	this work
$PrSO_3H$-KIT-6-100	6.2	27.6	41.0	41	this work
$PrSO_3H$-KIT-6-120	7.0	39.3	50.9	60.7	this work
$PrSO_3H$-SBA-15-6	6	23.2	na	23.4	33
$PrSO_3H$-SBA-15-8	8	32.9	na	55.2	33
$PrSO_3H$-MM-SBA-15-4	4/300[d]	55.4	na	35.6	32

[a]Conversion after 6 h reaction. [b]TOF based on NH_3 titration. [c]Calculated per S site (based on bulk S content obtained by TGA). [d]Bimodal macro-mesoporous hierarchical pore structure.

diffusion via tuning the relative mesopore channel length, diameter, and interconnectivity. Future work will also explore the impact of cografted hydrophobic groups, the use of stronger acid functionalities (e.g., phenyl sulfonic acid), and means to increase acid site loadings and overall yields in fatty acid esterification employing these interconnected catalyst support architectures.

4. CONCLUSIONS

The first pore-expanded KIT-6 sulfonic acid catalysts have been synthesized and applied to the esterification of fatty acids with methanol. $PrSO_3H$-KIT-6 hydrothermally aged at 80 °C exhibits strong TOF-enhancements in propanoic and hexanoic acid esterification over a SBA-15 sulfonic acid of similar pore diameter. This is attributed to improved mass transport arising via the interconnected pore network of small KIT-6 cubic crystallites, compared to the two-dimensional, non-interconnected pores of larger, elongated SBA-15 crystallites, and associated enhanced access to the active sulfonic acid sites. Pore accessibility becomes rate-limiting for lauric and palmitic acid esterification for 5 nm KIT-6 and SBA-15 frameworks; however, hydrothermal aging at 120 °C facilitates KIT-6 pore expansion up to 7 nm, enhancing esterification activity toward all C_3−C_{16} fatty acids over $PrSO_3H$-SBA-15, offering a 2-fold TOF-enhancement for lauric and palmitic acid esterification.

■ ASSOCIATED CONTENT

Supporting Information

Porosimetry of sulfonic acid catalysts, reaction profiles used to determine catalyst activity for the series of organic acids and leaching studies. This material is available free of charge via the Internet at http://pubs.acs.org.

■ AUTHOR INFORMATION

Corresponding Author

*E-mail: Wilsonk5@cardiff.ac.uk..

Present Address

[†]UCCS, University of Lille I, 59655 Villeneuve d'Ascq, Lille, France.

Funding

We thank the EPSRC for funding (EP/F063423/2). K.W. acknowledges The Royal Society for the award of an Industry Fellowship, and A.F.L. thanks the EPSRC for the award of a Leadership Fellowship (EP/G007594/2).

Notes

The authors declare no competing financial interest.

■ REFERENCES

(1) Armaroli, N.; Balzani, V. *Angew. Chem., Int. Ed.* **2007**, *46*, 52−66.
(2) *BP Energy Outlook 2030*; London, U.K., January 2011.
(3) Ma, F. R.; Hanna, M. A. *Bioresour. Technol.* **1999**, *70*, 1−15.
(4) Gryglewicz, S. *Bioresour. Technol.* **1999**, *70*, 249−253.
(5) European Committee for Standardization, Automotive fuels - Fatty acid methyl esters (FAME) for diesel engines - Requirements and test methods. EN 14214:2008 (E)
(6) Directive 2003/30/EC of the European Parliament and of the Council of 8 May 2003 on the promotion of the use of biofuels or other renewable fuels for transport, *Official Journal of the European Union*.
(7) Melero, J. A.; Van Grieken, R.; Morales, G. *Chem. Rev.* **2006**, *106*, 3790−3812.
(8) Narasimharao, K.; Lee, A. F.; Wilson, K. *J. Biobased Mater. Bioenergy* **2007**, *1*, 19−30.
(9) Wilson, K.; Lee, A. F. *Catal. Sci. Technol.* **2012**, *2*, 884−897.
(10) Santacesaria, E.; Tesser, R.; Di Serio, M.; Guida, M.; Gaetano, D.; Agreda, A. G.; Cammarota, F. *Ind. Eng. Chem. Res.* **2007**, *46*, 8355−8362.
(11) Canakci, M.; Van Gerpen, J. *Trans. ASAE* **2001**, *44*, 1429−1436.
(12) Ni, J.; Meunier, F. C. *Appl. Catal., A* **2007**, *333*, 122−130.
(13) Lopez, D. E.; Goodwin, J. G., Jr.; Bruce, D. A.; Furuta, S. *Appl. Catal., A* **2008**, *339*, 76−83.
(14) Xiao-Rong, C.; Yi-Hsu, J.; Chung-Yuan, M. *J. Phys. Chem. C* **2007**, *111*, 18731−18737.
(15) Alsalme, A.; Kozhevnikova, E. F.; Kozhevnikov, I. V. *Appl. Catal., A* **2008**, *349*, 170−176.
(16) Leng, Y.; Wang, J.; Zhu, D.; Wu, Y.; Zhao., P. *J. Mol. Catal. A* **2009**, *313*, 1−6.
(17) Dufaud, V.; Lefebvre, F.; Niccolaic, G. P.; Mimoun, A. *J. Mater. Chem.* **2009**, *19*, 1142−1150.
(18) Rao, K. N.; Brown, D. R.; Lee, A. F.; Newman, A. D.; Siril, P. F.; Tavener, S. J.; Wilson, K. *J. Catal.* **2007**, *248*, 226−234.
(19) Pesaresi, L.; Brown, D. R.; Lee, A. F.; Montero, J. M.; Williams, H.; Wilson, K. *Appl. Catal., A* **2009**, *360*, 50−58.
(20) López, D. E.; Suwannakarn, K.; Bruce, D. A.; Goodwin, J. G., Jr. *J. Catal.* **2007**, *247*, 43−50.
(21) Ngaosuwan, K.; Mo, X.; Goodwin, J. G., Jr.; Praserthdam, P. *Appl. Catal., A* **2010**, *380*, 81−86.
(22) Ngaosuwan, K.; Mo, X.; Goodwin, J. G., Jr.; Praserthdam, P. *Top. Catal.* **2010**, *53*, 783−794.
(23) Rao, K. N.; Sridhar, A.; Lee, A. F.; Tavener, S. J.; Young, N. A.; Wilson, K. *Green Chem.* **2006**, *8*, 790−797.
(24) Melero, J. A.; Iglesias, J.; Morales, G. *Green. Chem.* **2009**, *11*, 1285−1308.
(25) Wilson, K.; Clark, J. H. *Pure Appl. Chem.* **2000**, *72*, 1313−1319.
(26) Lee, A. F.; Wilson, K. Sol−gel sulfonic acid silicas as catalysts. In *Handbook of Green Chemistry - Green Catalysis*; Anastas, P. T., Crabtree, R. H., Eds.; Wiley-VCH: Weinheim, Germany, 2009; Chapter 2.
(27) Lu, Y.; Guo, Y.; Wang, Y.; Liu, X.; Wang., Y.; Guo, Y.; Zhang, Z.; Lu, G. *Microporous Mesoporous Mater.* **2008**, *114*, 507−510.
(28) Miao, S.; Shanks, B. H. *Appl. Catal., A* **2009**, *359*, 113−120.
(29) Mbaraka, I. K.; Shanks, B. H. *J. Catal.* **2006**, *244*, 78−85.
(30) Miao, S.; Shanks, B. H. *J. Catal.* **2011**, *279*, 136−143.
(31) Zhang, Q.; Chang, J.; Wang, T.; Xu, Y. *Energy Fuels* **2006**, *20*, 2717−2720.
(32) Dhainaut, J.; Dacquin, J. P.; Lee, A. F.; Wilson, K. *Green Chem.* **2010**, *12*, 296−303.

(33) Dacquin, J. P.; Lee, A. F.; Pirez, C.; Wilson, K. *Chem. Commun.* **2012**, *48*, 212−214.
(34) Kleitz, F.; Choi, S. H.; Ryoo, R. *Chem. Commun.* **2003**, 2136−2137.
(35) Vinu, A.; Gokulakrishnan, N.; Balasubramanian, V. V.; Alam, S.; Kapoor, M. P.; Ariga, K.; Mori, T. *Chem.—Eur. J.* **2008**, *14*, 11529−11538.
(36) Parlett, C. M. A.; Bruce, D. W.; Hondow, N.; Lee, A. F.; Wilson, K. *ACS Catal.* **2011**, *1*, 636−640.
(37) Calin, N.; Galarneau, A.; Cacciaguerra, T.; Denoyel, R.; Fajula, F. *C. R. Chim.* **2010**, *13*, 199−206.
(38) Zhao, D.; Huo, Q.; Feng, J.; Chmelka, B. F.; Stucky, G. D. *J. Am. Chem. Soc.* **1998**, *120*, 6024−6036.
(39) Kleitz, F.; Choi, S. H.; Ryoo, R. *Chem. Commun.* **2003**, 2136−2137.
(40) Kleitz, F.; Berube, F.; Guillet-Nicolas, R.; Yang, C. M.; Thommes, M. *J. Phys. Chem.* **2010**, *114*, 9344−9355.
(41) Kim, T. W.; Kleitz, F.; Paul, B.; Ryoo, R. *J. Am. Chem. Soc.* **2005**, *127*, 7601−7610.
(42) Kleitz, F.; Berube, F.; Guillet-Nicolas, R.; Yang, C. M.; Thommes, M. *J. Phys. Chem. C* **2010**, *114*, 9344−9355.
(43) Hamoudi, S.; Royer, S.; Kaliaguine, S. *Microporous Mesoporous Mater.* **2004**, *71*, 17−25.
(44) Mueller, R.; Kammler, H. K.; Wegner, K.; Pratsinis, S. E. *Langmuir* **2003**, *19*, 160−165.
(45) Liu, Y.; Lotero, E.; Goodwin, J. G., Jr. *J. Catal.* **2006**, *243*, 221−228.
(46) Lilja, J.; Murzin, Y.-D.; Salmi, T.; Aumoa, J.; Mäki-Arvela, P.; Sundell, M. *J. Mol. Catal. A* **2002**, *182−183*, 555−563.
(47) Charton, M. *J. Org. Chem.* **1976**, *41*, 2217−2220.
(48) Siril, P. F.; Shiju, N. R.; Brown, D. R.; Wilson, K. *Appl. Catal., A* **2009**, *364*, 95−100.
(49) Miao, S.; Shanks, B. H. *J. Catal.* **2011**, *279*, 136−143.
(50) Dacquin, J. P.; Cross, H. E.; Brown, D. R.; Duren, T.; Williams, J. J.; Lee, A. F.; Wilson., K. *Green Chem.* **2010**, *12*, 1383−1391.
(51) Chen, S.-Y.; Yokoi, T.; Tang, C.-Y.; Jang, L.-Y.; Tatsumi, T.; Chan, J. C. C.; Cheng, S. *Green Chem.* **2011**, *13*, 2920−2930.
(52) Wainwright, S. G. Ph.D. Thesis, University of York, York, U.K., 2011.